ChemComm

Synthesis and characterization of a bimetallic americium(III) pyrithionate coordination complex

Journal:	*ChemComm*
Manuscript ID	CC-COM-06-2022-003352.R1
Article Type:	Communication

COMMUNICATION

Synthesis and characterization of a bimetallic americium(III) pyrithionate coordination complex

Received 00th January 20xx,
Accepted 00th January 20xx

DOI: 10.1039/x0xx00000x

Zachary K. Huffman,[a] Joseph M. Sperling,[a] Cory J. Windorff,[a,b] Brian N. Long,[a] Lucas Cordova,[a] Harry Ramanantoanina,[c] Cristian Celis-Barros,*[a] Thomas E. Albrecht-Schönzart*[a]

The aqueous reaction of sodium pyrithione, (Na)mpo, with $^{243}AmCl_3 \bullet nH_2O$ yields a dimerized complex, $[^{243}Am(mpo)_2(\mu\text{-}O\text{-}mpo)(H_2O)]_2 \bullet 3H_2O$. This compound is compared with isostructural lanthanide pyrithionates, where dimerization across the 4*f*-block is observed to be dependent upon the size of the cation. Unlike most reported Am(III) UV-visible absorption spectra, $[^{243}Am(mpo)_2(\mu\text{-}O\text{-}mpo)(H_2O)]_2 \bullet 3H_2O$ shows significant splitting in the fingerprint excitations. This is attributed to a unique ligand-field environment, where the Am–mpo bonds possess different bonding compared to the Nd(III) analog because of increasing covalent interactions.

In recent years, actinide research has been subject of increased interest not only from a fundamental perspective but also because of their potential in clean energy, catalysis, and radiotherapy.[1–7] However, the inherent challenges associated with working with these elusive elements bottleneck these efforts. Currently, the field has reached a point where combining the knowledge of the intrinsic properties of the metal with tailored ligands is paramount. As it is known, these elements exhibit unique properties because of the gradual occupation of the 4*f* and 5*f* orbitals.[8,9] At the same time, the similarity in chemical behavior makes differentiation between most of these elements with electronic differences alone untenable. This necessitates the need for tunable ligand motifs that are capable of either selective ion recognition or the enhancement of specific chemical or structural properties.

Aromatic hydroxamates such as 2-hydroxypyridine N-oxide (HOPO) have been heavily utilized in the sequestration of *f*-elements, and several *f*-element hydroxypyridonate complexes have been reported to have high stability constants.[7,10–12] The coordination of the hydroxamate moiety with a metal center is characterized by a bidentate five-membered ring as shown in **Fig. 1A**. 2-mercaptopyridine N-oxide (mpo, **Fig. 1B**) is a thioamide bidentate ligand that is structurally similar to HOPO, both of which feature an amine-oxide moiety. The prototrope, mpo exhibits tautomerism analogous to that observed in HOPO, although the thione tautomer is favored over the thiol form. Despite a breadth of reported mpo transition metal chemistry, there are but a handful of reported *f*-element pyrithionate complexes.[13–20] Emerging evidence shows that soft donor atoms like sulfur exhibit increased covalent interactions with a variety of 5*f* complexes, where the 5*f* orbitals are engaged in orbital mixing with the sulfur 3*p* orbitals.[8,21] This effect is pronounced for later actinides because of a better energy match between these orbitals.[22] Although there is potential for soft donor ligands to play a substantial role in the separation of trivalent actinides, 2-mercaptopyridine N-oxide has largely been overlooked in the chelation of *f*-elements.[8,23,24] Of particular interest is americium (Am) owing to the well-known issue in separating it from curium (Cm) and most lanthanides because of their predominately trivalent nature and nearly identical effective ionic radii.[25] Herein, we report the aqueous complexation of Am^{3+} and lanthanides La-Lu (except Ce, Pm) by mpo, which display a size-selective dimerization across the *f*-block and consisting of rather unique features in the absorption spectrum of the Am complex.

Lanthanide pyrithionate complexes **1-Ln** (Ln = Pr, Nd, Sm, Eu, Gd, Tb) and **2-Ln** (Ln = Dy, Ho, Er, Yb, Lu) were prepared using two different starting materials. Three equivalents of Na(mpo) in water were combined with the corresponding lanthanide chloride or nitrate in water and slow evaporation of

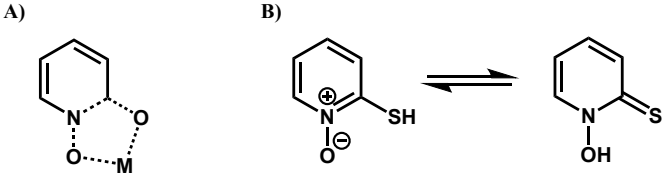

Figure 1: A) Five-membered hydroxamate ring utilizing HOPO. B) Tautomerization exhibited by 2-mercaptopyridine N-oxide.

[a] *Department of Chemistry and Biochemistry, Florida State University, 95 Chieftan Way, Tallahassee, Florida 32306, United States.*
[b] *Department of Chemistry and Biochemistry, New Mexico State University, MSC 3C, PO Box 3001, Las Cruces, New Mexico 88003, United States.*
[c] *Karlsruhe Institute of Technology, Institute for Nuclear Waste Disposal (INE), P.O. Box 3640, D-76021 Karlsruhe, Germany.*
Electronic Supplementary Information (ESI) available: [details of any supplementary information available should be included here]. See DOI: 10.1039/x0xx00000x

the resulting solutions yielded X-ray quality crystals within 1-2 days (see ESI for details). Among the larger lanthanides Pr-Tb (except Pm), **1-Ln** crystallize as dimeric structures [Ln(mpo)$_2$(μ-O-mpo)(H$_2$O)]$_2$ in the monoclinic space group $P2_1/c$ where each metal center exhibits 8-coordinate distorted dodecahedral geometry. The metal center is coordinated by one water molecule and three bidentate pyrithionate ligands where the third pyrithionate ligand features a bridging μ-oxygen to the adjacent metal center. The smaller lanthanides Dy-Lu, crystallize as monomeric structures Ln(mpo)$_3$(H$_2$O)$_2$, **2-Ln**, in the triclinic space group $P\bar{1}$. **2-Ln** exhibits an 8-coordinate distorted dodecahedral geometry and is bound by three bidentate pyrithionate ligands and two water molecules (**See ESI for structures**).

While **1-La** was successfully isolated as a crystalline product, the products were unsuitable for single crystal XRD. The reaction between cerium and mpo following the same procedure did not result in isolable material.

Figure 2: Averaged bond distances of selected *f*-element pyrithionate complexes.

For the dimerization between **1-Ln** and **2-Ln**, a similar change in stoichiometry has been observed using other ligands and this phenomenon is thought to be correlated to a decreasing ionic radius of the cation.[26,27] HOPO specifically has been reported to exhibit this, with a series of tetrakis complexes with bridging alkali ions reported for the lanthanides with a similar transition point to monomeric complexes occurring at Gd.[26] Appropriately, the average metal-oxygen bond lengths in both **1-Ln** and **2-Ln** are observed to decrease and widely follow the lanthanide contraction, **Fig. 2** and **Tables S2** and S**3**.

To investigate this systematic trend among the predominately trivalent actinides, **1-Am** was prepared in a manner similar to **1-Ln** and **2-Ln** by combining AmCl$_3$•nH$_2$O with 3 equivalents Na(mpo) in water. Slow evaporation of the solution for 48 hours yielded yellow X-ray quality crystals. **1-Am** crystallizes as a dimeric structure, [Am(mpo)$_2$(μ-O-mpo)(H$_2$O)]$_2$ in the triclinic space group $P\bar{1}$ with a 8-coordinate distorted dodecahedral geometry, **Fig. 3**.

There is just one example of an 8-coordinate Am structure that features Am-O$_{N\text{-oxide}}$ bonds, specifically [Am(2,6-[Ph$_2$P(O)CH$_2$]$_2$C$_5$H$_3$–NO))$_2$(NO$_3$)][2(NO$_3$)].[28] The average Am-O$_{N\text{-oxide}}$ bond distance (2.506(10)Å) are slightly longer than those found in **1-Am,** however this might be best explained by steric hindrance of the tridentate ligand as the reported Nd analog, [Nd(2,6-[Ph$_2$P(O)CH$_2$]$_2$C$_5$H$_3$–NO))$_2$(NO$_3$)][2(NO$_3$)], contains similar M-O$_{N\text{-oxide}}$ bond distances to that of the Am compound.[29] There are no reported Am compounds featuring simultaneously both Am-O$_{N\text{-oxide}}$ and Am-S bonds. Despite this, **1-Am** can be compared to the isostructural **1-Nd** analogue which is similar in terms of the 8-coordinate ionic radius, 1.09 Å and 1.109 Å, respectively.[30] The average M-O$_{mpo}$ bond distance in **1-Am** (2.398(2) Å) are nearly identical to those in **1-Nd** (2.393(2) Å), as is often the case for systems comparing Nd^{3+} and Am^{3+}, however the average Am-S bond distance (2.903(2)Å) is considerably shorter than that of **1-Nd** (2.934(1) Å).[31] This 0.031(2) Å difference is much larger than the 0.019 Å difference in ionic radii between 8-coordinate Nd^{3+}/Am^{3+}.[30] From the roughly 40 reported single crystal structures containing Am^{3+}, **1-Am** represents only the fourth case of crystallographically measured Am-S bonds. The average Am-S bond distance compares favorably with the other three examples, namely that of Am(S$_2$CNEt$_2$)$_3$(N$_2$C$_{12}$H$_8$) (2.86(4) Å), (NBu$_4$)Am[S$_2$P(^{t}Bu$_2$C$_{12}$H$_6$)]$_4$ (2.921(3) Å), and [Am(S$_2$P(OEt)$_2$)$_4$]$^{1-}$ (2.912(1) Å).[32–34]

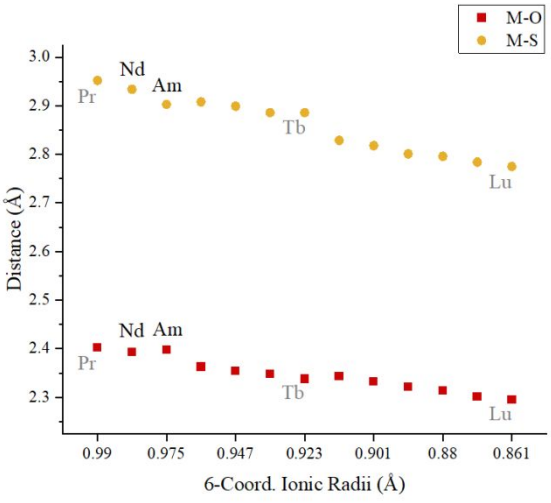

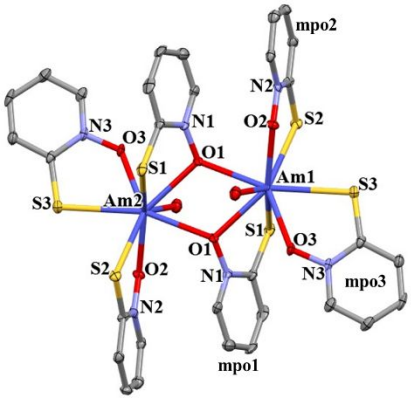

Figure 3: Thermal ellipsoids (50% probability) for [Am(mpo)$_2$(μ-O-mpo)(H$_2$O)]$_2$ where solvent molecules and hydrogens are omitted for clarity.

Among the dimers **1-Ln**, the average Ln-S and Ln-O$_{mpo}$ bond lengths decrease across the series congruent with the lanthanide contraction, **Table S2**. The longest M-O$_{mpo}$ bonds in both **1-Am** and **1-Ln** are found within the pyrithionate ligand that contains the longest M-S bond, and conversely the shortest M-O$_{mpo}$ bonds are found in the same pyrithionates as the shortest M-S bonds. The μ-O bonds found in **1-Ln** are symmetric, however this is not the case in **1-Am**: M-S bonds are still longest across bridging pyrithionates like **1-Ln**, however the μ-O bonding is asymmetric across metal centers with a difference of 0.05 Å, **Table S29**.

Aside from the asymmetric μ-O bonding between adjacent metals centers in **1-Am**, discernable differences for the change

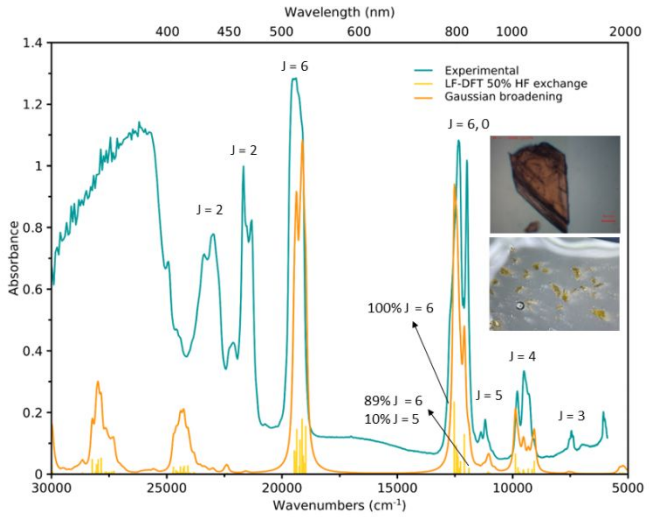

Figure 4: Experimental and LF-DFT calculated solid-state UV-vis/NIR absorption spectra of **1-Am**. Crystal used for experimental collection shown in inset.

in crystal class from $P2_1/c$ to $P\bar{1}$ are perhaps more obvious when examining the crystal packing. **1-Am** and **1-Ln** both exhibit displaced π-stacking between bridged pyrithionate ligands and an adjacent, terminal pyrithionate ligand in the same molecule. The bridged pyrithionate ligand also has sandwich π-stacking with a bridged pyrithionate ligand in the neighboring molecule, forming a 4-ring stack between two discrete molecules of **1-Am** and **1-Ln**, respectively. Moreover, terminal pyrithionate ligands in **1-Am** feature displaced π-stacking with terminal pyrithionate ligands in neighboring molecules. These same terminal pyrithionate ligands have no appreciable π-stacking in **1-Ln**. The π-stacked pyrithionate ligands in **1-Am** and **1-Ln** are further distinguishable by the shorter centroid-centroid distances between adjacent rings found in **1-Am** compared to **1-Ln** which results in tighter crystal packing, **Figure S13**. Finally, differences in crystallinity are further observed with the presence of three outer sphere water molecules in **1-Am** which are absent in **1-Ln.**

Solid state UV-vis spectroscopy was collected to additionally characterize these complexes (**1-Ln** and **2-Ln**, see ESI). For further analysis of **1-Am**, we relied on the three features that are the fingerprint of the Am^{3+} ion, namely those *f-f* transitions conventionally identified as $^7F_0 \rightarrow {}^5L_6$ (515.7 nm), $^7F_0 \rightarrow {}^7F_6$ (810.24, 834.74 nm), and $^7F_0 \rightarrow {}^7F_4$ (1021.24, 1052.43 nm) as shown in **Figure 4**. Notably, the $^7F_6$ and $^7F_4$ transitions have evident splitting. Other Am-S containing complexes also exhibit splitting for these transitions, specifically $AsPh_4[Am(S_2P(OEt)_2)_4]$ in the $^7F_4$ transition where splitting in the latter molecule spans nearly twice the range that the splitting does in **1-Am**.[33] Furthermore, splitting in the $^7F_6$ transition in $(NBu_4)Am[S_2P(^tBu_2C_{12}H_6)]_4$ is significantly smaller compared to **1-Am**.[32] Even with few reported solid-state UV-vis spectra of Am^{3+} complexes, splitting in both the $^7F_6$ and $^7F_4$ transitions is seldomly seen at the same time.[33]

The absorption spectrum of **1-Am** was further rationalized by means of the ligand field density functional theory (LFDFT) approximation, see ESI.[35] It is noteworthy to mention that in the intermediate coupling scheme, which is where lanthanide and more importantly actinides lie, the composition of the wavefunctions can be extremely complex. Thus, the wavefunction analysis will be focus on the J = 0 ⟶ J' = 4, 5, 0, 6 transitions (Figure 4). The ground state of Am(III) complexes corresponds to a J = 0 manifold with mainly $^7F_0$ character (over 75% in most cases), but in **1-Am** decreases significantly to 50% (Table S33). As mentioned above, the J = 0 ⟶ J' = 4, 6 transitions are two of the Am^{3+} "fingerprints" because these correspond to induced electric dipole allowed transitions (ΔS = 0, ΔL and ΔJ = 2, 4, 6 for a J = 0 ground state). This explains the higher intensity of the bands centred at *ca.* 800 nm (J = 6) and 1050 nm (J = 4). Conversely, the J = 5 band is more difficult to recognize and sometimes not even present as is the case of $(PPh_4)_3AmCl_6$.[36] The J = 0 band is even harder to see because of the forbidden nature of the J = 0 ⟶ J' = 0 transition in addition to the potential masking due to the more intense J = 6 band, which is the case of **1-Am**. The separation of this transition from the J = 6 manifold depends strongly on the metal–ligand interaction (Figure S22). As the wavefunctions of the J = 5, 6, 0 manifolds are projected onto their J-components, it allowed us to see how the J = 5 states mix with the J = 6 manifold. This explains the increased intensity observed compared to what is typically expected for these transitions. Similarly, spin-orbit states sharing J = 5 character in the J = 6 manifold present decreased intensities as shown in Figure 4. Thus, the structural and spectroscopic data suggests a rather unusual Am-mpo interaction.

The bonding of **1-Nd**, **1-Eu**, and **1-Am** was investigated through the Natural Localized Molecular Orbital (NLMO) approximation. Figures S20 and S21 show the NLMOs describing the Am–mpo and Nd–mpo interactions. An inspection of these NLMOs suggest significant differences between Am–S and Ln–S bonds, despite one NLMO common to all M–S bonds was found (**Figure S19**). This particular NLMO is the main contributor to the total NLMO-Bond Indices (BI) in every M–S σ–bond except in the case of Am–S3. The terminal mpo ligand, whose M–L bonds are stronger according to the predicted BIs (**Table S30**), display a strong σ–type interaction (Am–S3, BI = 0.31) that accounts for ~ 70% of the total NLMO-BI (0.433). This NLMO has 15% Am contribution that is the highest observed of all Am – L in the complex and higher than other Am–S bonds reported with a sizable 5*f* contribution (42% of the hybrid contribution).[37] Similarly, the Am–S2 bond also displays a unique interaction but weaker (BI = 0.13) compared to the Am–S3 σ–NLMO owing to its π nature. It accounts for only ~ 38% of the total NLMO-BI (0.348) with a highly polar character (7% Am). Despite the polar nature, 62% of the Am hybrid contribution corresponds to 5*f* orbitals that highlight its importance in the M–L interaction. Owing to the differential radial extent of 5*f* versus 4*f* orbitals, it seems plausible that the unusually high 5*f* orbital contributions are the reason why these unique NLMOs are not observed in **1-Ln**.

In conclusion, lanthanide and americium pyrithionate compounds have been prepared using a salt metathesis reaction. A comparison of the isostructural **1-Nd**, **1-Eu**, and **1-Am** shows that the Am-S bonds are much shorter than the Nd-S bonds, despite the similar ionic radii. The bond length

difference implies the presence of stronger bonding interactions in **1-Am**. The origin of these stronger interactions in **1-Am** might lie in the particular electronic structure of the mpo ligand, with evident flexibility toward electronic rearrangement upon coordination. Such a concept could be exploited for improving chemical selectivity toward actinides such as Am^{3+} over Ln^{3+}. This uniqueness is also highlighted in the unusual UV-vis-NIR absorption spectrum of **1-Am**, where the sensitive $^7F_0 \rightarrow {}^7F_6$ and $^7F_0 \rightarrow {}^7F_4$ transitions display a significant splitting with respect to previously reported Am^{3+} spectra.

Support for this research was provided as part of the Center for Actinide Science and Technology (CAST) funded by the U.S. Department of Energy, Office of Science, Office of Basic Energy Sciences, under Award Number DE-SC0016568.

Conflicts of interest

There are no conflicts to declare.

Notes and references

1 Grimes, R. W.; Konings, R. J. M.; Edwards, L. *Nature Mat*. 2008, **7**, 683-685.
2 Hill, D. J. *Nature.* 2008, **488**, 294-303.
3 Chu, S.; Majumdar, A. *Nature*. 2012, 294
4 Batrice, R. J.; Kefalidis, C. E.; Maron, L.; Eisen, M. S. *J. Am. Chem. Soc.* 2016, *138*, 2114-2117.
5 Arnold, P. L.; Turner, Z. R. *Nat. Rev. Chem*. 2017. **1**, 2, 1.
6 Weiss, C. J.; Marks, T. J. *Dalton Trans.* 2010, **39**, 6576-6588.
7 Kelley, M. P.; Deblonde, G. J. P.; Su, J.; Booth, C. H.; Abergel, R. J.; Batista, E. R.; Yang, P. *Inorg. Chem.* 2018, **57**, 5352-5363.
8 Neidig, M. L.; Clark, D. L.; Martin, R. L. *Coord. Chem. Rev*. 2013, **257**, 394-406.
9 Choppin, G. R. Covalency in *F*-Element Bonds. *J. Alloys Compd.* 2002, **344**, 55-59.
10 Abergel, R. J.; Durbin, P. W.; Kullgren, B.; Ebbe, S. N.; Xu, J.; Chang, P. Y.; Bunin, D. I.; Blakely, E. A.; Bjornstad, K. A.; Rosen, C. J.; Shuh, D. K.; Raymond, K. *Health Physics*; 2010; **99**, 401-407.
11 Moore, E. G.; Jocher, C. J.; Xu, J.; Werner, E. J.; Raymond, K. N. *Inorg. Chem.* 2007, **46**, 5468-5470.
12 Durbindagger, P. W.; Kullgren, B.; Xu, J.; Raymond, K. N. *Int. J. Radiat. Bio.* 2000, **76**, 199-214
13 Karayannis, N. M.; Pytlewski, L. L.; Mikulski, C. M. *Coord. Chem. Rev.* 1973, **11**, 93-159.
14 Das, A.; Han, Z.; Brennessel, W. W.; Holland, P. L.; Eisenberg, R. *ACS Catalysis.* 2015, **5**, 1397-1406.
15 Ngcephe, A. M.; Sinha, M. K.; Purcell, W. *J. Mol. Struct.* 2020, **1199**, 127009.
16 Chen, X.; Hu, Y.; Wu, D.; Weng, L.; Kang, B. *Polyhedron*. 1991, **10**, 2651-2657.
17 Zhang, G. *Cryst. Eng. Comm.* 2013, **15**, 6453-6456.
18 West, D. X.; Frank, C. A. *J. Inorg. Nucl. Chem.* 1979, **41**, 49-53.
19 Xiong, R.-G.; Zuo, J.-L.; You, X.-Z.; Huang, X.-Y. *Polyhedron* 1996, **15**, 3321.
20 Casellato, U.; Vigato, P. A.; Tamburini, S.; Graziani, R.; Vidali, M. *Inorganica Chim. Acta.* 1983, **72**, 141-147.
21 Minasian, S. G.; Keith, J. M.; Batista, E. R.; Boland, K. S.; Clark, D. L.; Conradson, S. D.; Kozimor, S. A.; Martin, R. L.; Schwarz, D. E.; Shuh, D. K.; Wagner, G. L.; Wilkerson, M. P.; Wolfsberg, L. E.; Yang, P. *J. Am. Chem. Soc.* 2012, **134**, 5586-5597.
22 Kelley, M. P.; Su, J.; Urban, M.; Luckey, M.; Batista, E. R.; Yang, P.; Shafer, J. C. *J. Am. Chem. Soc.* 2017, **139**, 9901-9908.
23 Klaehn, J. R.; Peterman, D. R.; Harrup, M. K.; Tillotson, R. D.; Luther, T. A.; Law, J. D.; Daniels, L. M. *Inorganica Chim. Acta* 2008, ***361***, 2522-2532.
24 Vats, B. G.; Gamare, J. S.; Kannan, S.; Pius, I. C.; Noronha, D. M.; Kumar, M. *Inorganica Chim. Acta* 2017, **467**, 1-6.
25 Street, K.; Seaborg, G. T. *J. Am. Chem. Soc.* 1950, **72**, 2790
26 Tedeschi, C.; Azéma, J.; Gornitzka, H.; Tisnès, P.; Picard, C. A *Dalton Trans.* 2003, **9**, 1738-1745.
27 Goodgame, D. M. L.; Hill, S. P. W.; Williams, D. J. *Inorg. Chim. Acta* 1997, **272**, 131-140.
28 Corbey, J. F.; Rapko, B. M.; Wang, Z.; McNamara, B. K.; Surbella, R. G.; Pellegrini, K. L.; Schwantes, J. M. *Inorg. Chem.* **57**, 2278-2287.
29 Galley, S. S.; Sperling, J. M.; Windorff, C. J.; Zeller, M.; Albrecht-Schmitt, T. E.; Bart, S. C. *Organometallics* 2019, **38**, 606-609.
30 Shannon, R. D. ; *Acta Cryst. A*. 1976. **A32**, 751-767.
31 Goodwin, C. A. P.; Schlimgen, A. W.; Albrecht-Schönzart, T. E.; Batista, E. R.; Gaunt, A. J.; Janicke, M. T.; Kozimor, S. A.; Scott, B. L.; Stevens, L. M.; White, F. D.; Yang, P. *Angew. Chem. Int. Ed.* 2021, **60**, 9459-9466.
32 Cross, J. N.; Macor, J. A.; Bertke, J. A.; Ferrier, M. G.; Girolami, G. S.; Kozimor, S. A.; Maassen, J. R.; Scott, B. L.; Shuh, D. K.; Stein, B. W.; Stieber, S. C. E. *Angew. Chem. Int. Ed.* 2016, **128**, 12947-12951.
33 Greer, R. D. M.; Celis-Barros, C.; Sperling, J. M.; Gaiser, A. N.; Windorff, C. J.; Albrecht-Schönzart, T. E. *Inorg. Chem.* 2020, **59**, 16291-16300.
34 Cary, S. K.; Su, J.; Galley, S. S.; Albrecht-Schmitt, T. E.; Batista, E. R.; Ferrier, M. G.; Kozimor, S. A.; Mocko, V.; Scott, B. L.; van Alstine, C. E.; White, F. D.; Yang, P. *Dalton Trans.* 2018, **47**, 14452-14461.
35 Ramanantoanina, H.; Urland, W.; Cimpoesu, F.; Daul, C. *Phys. Chem. Chem. Phys.* 2013, 15, 13902-13910.
36 Wang, C.; Wu, Q. Y.; Kong, X. H.; Wang, C. Z.; Lan, J. H.; Nie, C. M.; Chai, Z. F.; Shi, W. Q. *Inorg. Chem.* 2019, **58**, 10047-10056.
37 Cross, J. N.; Su, J.; Batista, E. R.; Cary, S. K.; Evans, W. J.; Kozimor, S. A.; Mocko, V.; Scott, B. L.; Stein, B. W.; Windorff, C. J.; Yang, P. *J. Am. Chem. Soc.* 2017, **139**, 8667-8677.

